ChemComm
Chemical Communications

Accepted Manuscript

This article can be cited before page numbers have been issued, to do this please use: Y. Song, H. Yokoyama, Y. Shoji, H. Sakai, T. Hasobe and T. Fukushima, *Chem. Commun.*, 2026, DOI: 10.1039/D5CC06166K.

ROYAL SOCIETY OF CHEMISTRY

rsc.li/chemcomm

ChemComm

View Article Online
DOI: 10.1039/D5CC06166K

COMMUNICATION

Gate-opening cooperative methanol binding to multi-bladed benzenes bearing 1,2-diboryl functionality†

Received 00th January 20xx,
Accepted 00th January 20xx

DOI: 10.1039/x0xx00000x

Yunyi Song,[a,b] Hiromichi Yokoyama,[a,b] Yoshiaki Shoji,*[a,b,c] Hayato Sakai,[d] Taku Hasobe[d] and Takanori Fukushima*[a,b,c]

A newly synthesized multi-bladed benzene (2_o) bearing two oxaboraanthracenyl and two *N*-carbazolylphenyl units undergoes highly cooperative binding with multiple methanol molecules (Hill coefficient > 3.5), which is accompanied by significant changes in its absorption and fluorescence properties.

The incorporation of boron functionality into π-conjugated systems has been demonstrated to provide enhanced and intriguing emission properties due to the combined effects of p_π-π* interactions, polarization, and molecular orbital modulations.[1,2] Besides, the inherent Lewis acidity of the boron centre allows coordination of Lewis bases, such as F^-, amines, pyridines, and alcohols, which impairs the p_π-π* interactions, inducing substantial changes in the emission and electronic properties.[3a,4] Taking advantage of such coordination properties, a variety of boron-containing colorimetric and luminescent dyes capable of sensing Lewis bases have been developed.[3b,c] In this context, multi-boryl units having proximal boron centres are attractive as a component of functional dyes, since they may exhibit stronger coordination ability with Lewis bases due to increased Lewis acidity as well as a chelate effect.[5] For this application, a particular molecular design is required to ensure chemical stability, such as suppressing hydrolysis.

We have recently reported that 1,2-diborylacetylene (**1**, Fig. 1a), bearing planar 9-oxa-10-boraanthracene (OBAn) termini,[6] exhibits sufficient chemical stability to allow handling in air, while retaining the typical reactivity of alkynes. For example, compound **1** undergoes the Diels-Alder reaction with tetraphenylcyclopentadienone to yield 1,2-diboryl-3,4,5,6-tetraphenylbenzene ($\mathbf{2_H}$, Fig. 1a), a multi-bladed benzene

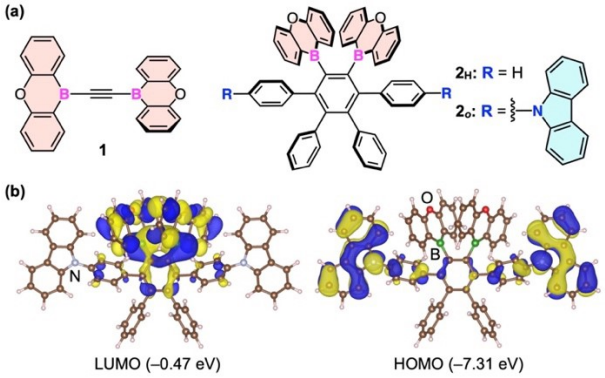

Fig. 1. (a) Chemical structures of 1,2-diborylacetylene (**1**) and 1,2-diboryl-3,4,5,6-tetraarylbenzenes ($\mathbf{2_H}$ and $\mathbf{2_o}$). (b) Kohn-Sham orbitals of $\mathbf{2_o}$. Energy levels are shown in parentheses.

featuring two adjacent OBAn groups.[6] Based on this finding, we newly designed $\mathbf{2_o}$ (Fig. 1a), in which carbazole units are introduced on the phenyl substituents at the 3,6-positions of the central benzene ring.

Density functional theory (DFT) calculations of $\mathbf{2_o}$ [the ωB97X-D/6-311G(d,p)//ωB97X-D/6-31G(d,p) level in vacuum, ESI†] predicted spatially separated frontier orbitals, in which the HOMO and LUMO located mainly on the carbazole and OBAn units, respectively (Fig. 1b). This orbital pattern fulfils one of the key requirements for the design of thermally activated delayed fluorescence (TADF) dyes,[1,7] whereas variable-temperature photoluminescence lifetime measurements of $\mathbf{2_o}$ in a polymer matrix showed no significant TADF features (Fig. S1, ESI†). However, we happened to find that multiple methanol (MeOH) molecules undergo complexation with $\mathbf{2_o}$ in a highly cooperative manner. Combined experimental and theoretical studies revealed that coordination of MeOH to the boron centres of $\mathbf{2_o}$ expands the internal cavity between the 1,2-OBAn units, thereby facilitating the binding of additional MeOH molecules. This "gate-opening-type" MeOH binding occurs in response to changes in the molar MeOH concentrations.

Compound $\mathbf{2_o}$ was obtained as a white powder in 50% yield by the Diels–Alder reaction between **1** and carbazole-appended tetraarylcyclopentadienone $\mathbf{3_o}$, conducted in molten benzophenone at 180 °C (ESI†). The chemical composition of $\mathbf{2_o}$ was confirmed by NMR and IR spectroscopy as well as high-

[a] Laboratory for Chemistry and Life Science, Institute of Integrated Research, Institute of Science Tokyo, 4259 Nagatsuta, Midori-ku, Yokohama 226-8501, Japan
E-mail: yshoji@res.titech.ac.jp (Yo.S.); fukushima@res.titech.ac.jp (T.F.)
[b] Department of Chemical Science and Engineering, School of Materials and Chemical Technology, Institute of Science Tokyo, 4259 Nagatsuta, Midori-ku, Yokohama 226-8501, Japan
[c] Research Center for Autonomous Systems Materialogy (ASMat), Institute of Integrated Research, Institute of Science Tokyo, 4259 Nagatsuta, Midori-ku, Yokohama 226-8501, Japan
[d] Department of Chemistry, Faculty of Science and Technology, Keio University, 3-14-1 Hiyoshi, Kohoku-ku, Yokohama, Kanagawa 223-8522, Japan
†Electronic Supplementary Information (ESI) available: Experimental details and analytical data. CCDC-2498455 ($\mathbf{2_o}$•MeCN). For ESI and crystallographic data, see DOI: 10.1039/x0xx00000x

resolution APCI-TOF mass spectrometry (ESI†). Compound **2$_o$** can be handled in air without special precautions, as in the case of **1**. Colourless prism-shaped single crystals of **2$_o$** suitable for single-crystal X-ray diffraction analysis were obtained by recrystallization from its acetonitrile (MeCN) solution (ESI†). In the crystal, **2$_o$** adopts a windmill-like geometry (Fig. S2, ESI†), with one MeCN molecule per **2$_o$**. The MeCN molecule is oriented with its methyl group toward the OBAn units, but shows no coordination to boron. Cyclic voltammetry (CV) of **2$_o$** in tetrahydrofuran at 298 K exhibited a reversible reduction wave at $E_{1/2}$ = –2.30 V *versus* the ferrocene/ferrocenium redox couple (Fig. S3a, ESI†). Unexpectedly, this potential is slightly more positive than that of **2$_H$** ($E_{1/2}$ = –2.35 V, Fig. S3b, ESI†) under identical conditions, despite the fact that **2$_o$** contains electron-donating carbazole units. This subtle yet counterintuitive trend prompted us to gain further insight into the relationship between the structures and electronic states for **2$_o$** and **2$_H$**.

In the optimized geometries at the ωB97X-D/6-311G(d,p)//ωB97X-D/6-31G(d,p) level in vacuum (ESI†), the LUMO level of **2$_H$** (–0.24 eV) is indeed higher than that of **2$_o$** (–0.47 eV), which is consistent with the results of CV measurements (Figs. S4a and S5, ESI†). Upon closer inspection, in both **2$_o$** and **2$_H$**, each OBAn unit is bent at the boron atom relative to the central benzene ring, bringing the two OBAn units into close proximity (Figs. S6 and S7, ESI†). We defined the bending angles as the dihedral angle between the mean planes of the OBAn rings and the trigonal boron planes. The values are 10.0° and 12.2° for **2$_o$** and **2$_H$**, respectively. The smaller bending angle in **2$_o$** suggests that the p_π-π* interactions within the OBAn units are greater in **2$_o$** than in **2$_H$**. Visualizing non-covalent interactions (NCI)[8] reveals the effect of the carbazole units adjacent to the OBAn units. Both **2$_o$** (Fig. S6a, ESI†) and **2$_H$** (Fig. S7a, ESI†) exhibit intramolecular van der Waals interactions between the windmill-arranged blade units. However, in **2$_o$**, additional CH–π interactions occur between the carbazole and the adjacent OBAn units, which may explain the higher planarity of the OBAn units in **2$_o$** compared to **2$_H$**. Furthermore, considering the large dihedral angles between the carbazole and the *ipso*-phenylene moieties in **2$_o$** (Fig. 1b), the carbazole functionality is expected to contribute to stabilization of the LUMO through an inductive effect, rather than to destabilization through π-donation *via* a mesomeric effect.

Figure 2a shows the absorption spectrum of **2$_o$** in toluene at 298 K (black solid curve), together with those of **2$_H$** (red dotted curve) and *N*-phenylcarbazole (*N*-PhCz) (blue dotted curve) for comparison. The first absorption band of **2$_o$** is observed as a shoulder at 360 nm, slightly red-shifted relative to that of **2$_H$** (λ_{max} = 355 nm). This band arises from an electronic transition involving the OBAn units (Fig. S4b, ESI†). In the shorter wavelength region, **2$_o$** displays absorption maxima at 343, 330 and 294 nm. These are attributed to the carbazole units, given the close similarity of the spectral pattern to that of *N*-PhCz (λ_{max} = 341, 327 and 285 nm). As shown in Fig. 2b, **2$_o$** in toluene (black solid curve) exhibits fluorescence at λ_{FL} = 460 nm (quantum yield Φ_F = 17.4%, lifetime τ = 5.8 ns, λ_{ex} = 294 nm).

In 1,2-dichloroethane (1,2-DCE), while the overall absorption maxima of **2$_o$** remains unchanged (Fig. 2a, green solid curve), the fluorescence maximum shows a bathochromic shift to 480 nm (Φ_F = 13.9%, τ = 18.8 ns, λ_{ex} = 294 nm), suggesting that the excited state of **2$_o$** possesses a significant polarized character (Fig. 2b). In a more polar solvent such as ethanol (EtOH), we observed dramatic changes in the absorption and fluorescence spectral shapes of **2$_o$**, both of which are almost identical to those of the reference compound, *N*-PhCz (Fig. 2c,d). These changes are attributed to coordination of EtOH to the boron centres, which suppresses the electronic transition involving the OBAn units, and instead, the locally excited (LE) state of the carbazole units predominantly contributes to the emission properties of **2$_o$**.

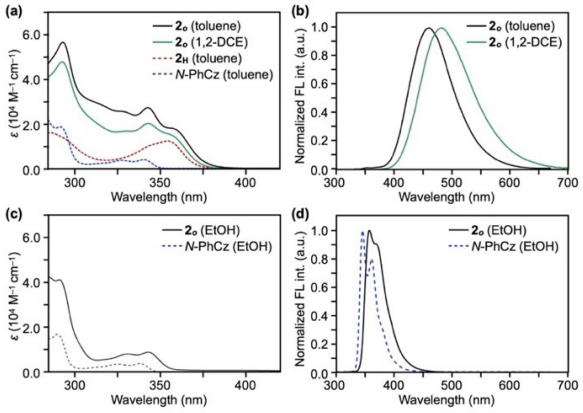

Fig. 2. Absorption and fluorescence spectra (1.0 x 10^{-5} M, 298 K). (a) Absorption spectra of **2$_o$** in toluene (black solid curve) and 1,2-DCE (green solid curve), and those of **2$_H$** (red dotted curve) and *N*-PhCz (blue dotted curve) in toluene. (b) Fluorescence spectra (λ_{ex} = 294 nm) of **2$_o$** in toluene (black solid curve) and 1,2-DCE (green solid curve). (c) Absorption spectrum of **2$_o$** in EtOH (black solid curve), along with that of *N*-PhCz in EtOH (blue dotted curve). (d) Fluorescence spectra (λ_{ex} = 294 nm) of **2$_o$** in EtOH (black solid curve) and *N*-PhCz in EtOH (blue dotted curve).

The above observation was unexpected to us, since the boron centre of **2$_o$** is sterically protected against hydrolysis. Indeed, upon addition of even 1.0 x 10^5 equivalents of dry EtOH to a 1,2-DCE solution of **2$_o$** (3.0 mL, 1.0 x 10^{-5} M) at 298 K resulted in almost no detectable changes in either absorption or fluorescence spectra (Fig. 3a,b). This indicates that the interactions between **2$_o$** and EtOH are very weak, such that significant coordination occurs only in pure EtOH. Interestingly, however, when dry MeOH (water content: <10 ppm) was titrated into a 1,2-DCE solution of **2$_o$** (3.0 mL, 1.0 x 10^{-5} M) under otherwise identical conditions to those used for EtOH, clear spectral changes were observed. Thus, the shoulder absorption peak around 360 nm due to the OBAn chromophore gradually decreased in intensity and eventually disappeared with isosbestic points (Fig. 3c). In the fluorescence spectra, the emission intensity at 480 nm decreased with increasing MeOH concentration, while a new band at 360 nm grew in intensity, showing an isoemissive point (Fig. 3d). Notably, the titration curves for both absorption and fluorescence (Fig. 3c–f) show that these spectra remain essentially unchanged within the initial titration range up to *ca*. 2.5 x 10^4 equivalents of MeOH. At higher MeOH concentrations, the response steeply increased in a sigmoidal manner. This spectral response indicates that the binding does not follow simple 1:1 stoichiometry but rather

involves a cooperative association of multiple MeOH with **2$_o$**. The spectral changes reached saturation after addition of *ca.* 2.0 x 10^5 equivalents of MeOH (*ca.* 240 μL).

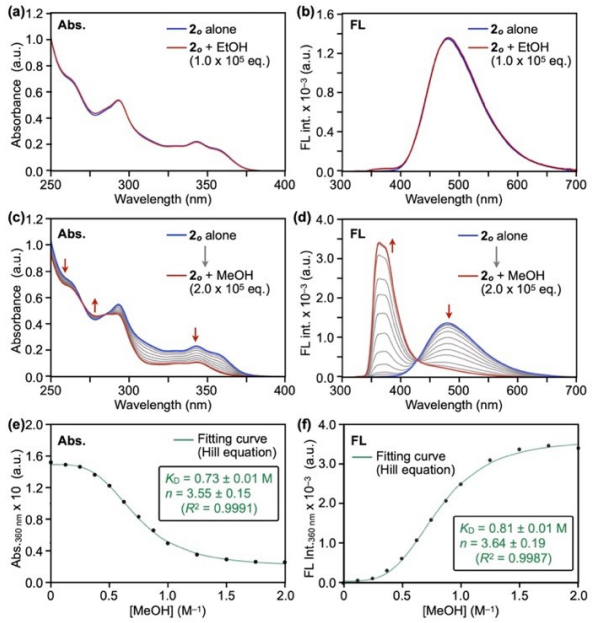

Fig. 3. Absorption and fluorescence spectra of **2$_o$** (1.0×10^{-5} M in 1,2-DCE at 298 K) upon titration with (a,b) EtOH (0.0–1.0 x 10^5 eq.) and (c,d) MeOH (0.0–2.0 x 10^5 eq.). Hill fittings of (e) the absorbance change at 360 nm and (f) fluorescence change at 360 nm using the data in panel (c) and (d), respectively.

To further analyze the association between **2$_o$** and MeOH, we fitted the titration data using a Hill model[9] (ESI†). As shown in Fig. 3e, the fitting curve (green) for the absorption changes agrees with the experimental plots (black, R^2 = 0.9991), giving an apparent dissociation constant of K_D = 0.73±0.01 M and a Hill coefficient of n = 3.55±0.15. This n value even exceeds those reported for the cooperative O_2 binding to hemoglobin ($n \leq 3.2$),[9] indicating pronounced positive cooperativity. The observed cooperativity is also evident in the Hill fitting of the fluorescence rise due to the carbazole chromophore at 360 nm (Fig. 3f, K_D = 0.81±0.01 M, n = 3.64±0.19). The titration profiles could not be fitted based on a stepwise association model but can be described as a two-state equilibrium (Fig. 3c,d). Consequently, parameter non-identifiability leads to significant uncertainty in each association constant. Nevertheless, the observed high Hill coefficients, which exceed the value expected for 1:2 stoichiometry, suggest that more than two MeOH molecules bind to **2$_o$** in a cooperative manner. Comparable Hill fitting results were also obtained (K_D = 1.06±0.02 M, n = 3.25±0.14) from UV-vis titration experiments performed at a tenfold higher concentration of **2$_o$** in 1,2-DCE (1.0×10^{-4} M) under otherwise identical conditions (Fig. S8, ESI†). In addition, NMR titration experiments carried out by adding MeOH to a CD_2Cl_2 solution of **2$_o$** (1.0×10^{-4} M) showed excellent agreement with the UV-vis titration results (K_D = 1.12±0.05 M, n = 3.57±0.12, Fig. S9, ESI†). These observations indicate that trace amounts of water, which could present as a trace impurity, have little influence on the titration results.

Another interesting observation is that **2$_H$** (Fig. 1a) also exhibits cooperative MeOH binding, although the cooperativity is lower than that observed for **2$_o$**. Upon titration with MeOH into a 1,2-DCE solution of **2$_H$** (3.0 mL, 1.0×10^{-5} M), the 355 nm absorption band of **2$_H$** gradually decreased (Fig. S10a), along with a reduction in fluorescence intensity at 470 nm, without the emergence of new emission band (Fig. S10b). The change in the absorbance of **2$_H$** also exhibits a sigmoidal feature, but the response is sluggish (Fig. S10c). Accordingly, a lower Hill coefficient (2.60±0.12) and a larger apparent K_D (1.33±0.04 M) were obtained than for **2$_o$**. Comparing the behavior of the MeOH titration between **2$_o$** and **2$_H$**, the presence of the carbazole units can enhance cooperativity for MeOH binding.

To gain insight into the initial binding steps that give rise to the observed cooperative behavior, as well as the effect of the carbazole units, we performed DFT calculations on 1:1 and 1:2 complexes of **2$_o$** and **2$_H$** with MeOH [the SMD(1,2-DCE)-ωB97X-D/6-311G(d,p)(C,H,B,N)/6-311+G(d,p)(O)//SMD(1,2-DCE)-ωB97X-D/6-31G(d,p)(C,H,B,N)/6-31+G(d,p)(O) level, ESI†]. Figure 4a shows the optimized geometries of 1:1 MeOH complexes of **2$_o$** (blue) and **2$_H$** (red), superimposed to highlight the differences in their structures. In the 1:1 complex of **2$_o$**, the O1 atom of MeOH coordinates asymmetrically to the two boron centres (B1–O1 = 1.733 Å, B2–O1 = 2.395 Å) with a slight elongation of the O1–H1 bond (0.971 Å) compared to that in free MeOH (0.963 Å). The more strongly bound B1 exhibits quaternization (the sum of the three C–B1–C angles Σ_{B1} = 344.8°), while the remaining B2 has an almost planar geometry (Σ_{B2} = 359.3°). This provides space for the incorporation of additional MeOH between the OBAn units (Fig. 4a, blue). In the 1:2 complex of **2$_o$**, the second MeOH molecule engages in hydrogen bonding with the first MeOH molecule, while the inter-OBAn spacing remains largely unchanged (Fig. 4b, blue). The O2–H2 bond in the second MeOH (0.967 Å) is slightly longer than that in free MeOH (0.963 Å) and shows a propensity for further association with MeOH.[4] For **2$_H$**, the optimized geometries around the OBAn units, including the coordinated MeOH molecules, are essentially identical to those obtained for **2$_o$** (Fig. 4a,b, red). Therefore, the difference between **2$_o$** and **2$_H$** observed in the titration experiment is not clear from these optimized structures.

However, the difference between **2$_o$** and **2$_H$** in MeOH binding can be seen in the calculated Gibbs free energies (Fig. 4c). At 298 K, the formation of the 1:1 complexes is largely endergonic for both **2$_o$** (ΔG = +8.00 kcal mol^{-1}) and **2$_H$** (ΔG = +8.62 kcal mol^{-1}), which is consistent with the observation that a large amount of MeOH is needed to shift the equilibrium towards complexation. Although the free energy change for forming the 1:1 complex is comparable for **2$_o$** and **2$_H$**, there is a clear energy difference between **2$_o$** (ΔG = +3.31 kcal mol^{-1}) and **2$_H$** (ΔG = +4.33 kcal mol^{-1}) in the second stage. Thus, the incorporation of a second MeOH is thermodynamically more favorable for **2$_o$** ($\Delta\Delta G$ = –4.69 kcal mol^{-1}) than for **2$_H$** ($\Delta\Delta G$ = –4.29 kcal mol^{-1}). The energy profile provides a reasonable explanation for the cooperative "gate-opening-type" MeOH binding behavior, as well as the observed difference in the titration experiments between **2$_o$** and **2$_H$**. We assume that the carbazole functionality stabilizes the opened-cavity geometry of the 1:1 MeOH complex for **2$_o$** through the CH–π interactions

with the adjacent OBAn units, thereby making the subsequent MeOH binding processes more favorable (Fig. 4).

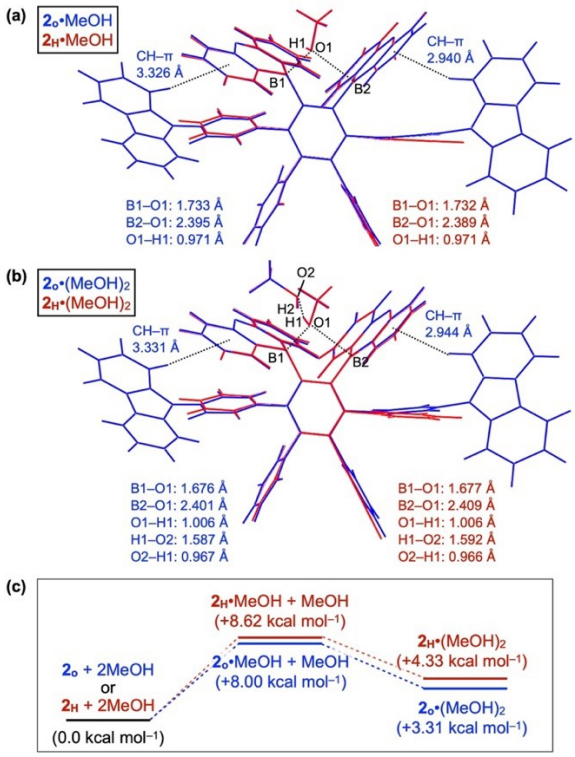

Fig. 4. Optimized geometries and selected interatomic distances of (a) 1:1 and (b) 1:2 MeOH complexes of $\mathbf{2_o}$ (blue) and $\mathbf{2_H}$ (red). The distances between the carbazole protons and the centroids of the phenylene rings in the OBAn units fall within the range of CH–π interactions. (c) Schematic diagram of the relative Gibbs free energies (298 K) of the calculated structures.

Finally, we examined the involvement of water in the complexation of MeOH with $\mathbf{2_o}$. Absorption and fluorescence spectra of $\mathbf{2_o}$ measured in water-saturated 1,2-DCE (water content: *ca.* 7 μL in 3 mL of 1,2-DCE)[10] are almost identical to those in dry 1,2-DCE (Fig. S11, ESI†), indicating that water alone scarcely induces a binding response. From titration experiments using a mixed solvent of MeOH/water (9/1 v/v), together with ESI-TOF mass spectrometric analysis of the titrated solution, MeOH was found to be the primary guest involved in the initial binding event, while water can serve as a competing guest in subsequent steps (Figs. S12 and S13, ESI†).

In summary, we have described the synthesis and properties of carbazole-appended multi-bladed benzene $\mathbf{2_o}$ featuring two adjacent OBAn units. This compound did not exhibit the TADF activity that we had initially anticipated, but we found that it undergoes an unexpected highly cooperative binding with MeOH, which is accompanied by changes in absorbance and the emergence of fluorescence from the locally excited state of the carbazole units. The dynamic range of MeOH concentration required to induce the cooperative binding is exceptionally large (up to several mol L^{-1}). Such properties have only previously been achieved in artificial systems by relying on porous molecular assemblies or polymeric systems having multiple binding sites.[11] This work demonstrates the potential of multi-boryl units as building blocks for the development of a new class of stimuli-responsive functional dyes.

This work was supported by a Grant-in-Aid for Transformative Research Areas (A) "Condensed Conjugation" (20H05868 to T.F. and 20H05869 to Yo.S.) from MEXT, JSPS KAKENHI (23H01945 and 25K21713 to Yo.S.), and the Research Program of "Five-star Alliance" in "NJRC Mater. & Dev.". Theoretical calculations were partially carried out using the TSUBAME4.0 supercomputer at Institute of Science Tokyo supported by the MEXT Project for the Academy for Convergence of Materials and Informatics (TAC-MI). Yu.S. is grateful to the support from JST SPRING, Japan (JPMJSP2180). H.Y. is grateful to the support from a Grant-in-Aid for JSPS Fellows (25KJ1239).

Conflicts of interest

There are no conflicts to declare.

Data availability

All experimental details and data supporting this article are available in the supplementary information (SI).

Notes and references

1 (a) H. Uoyama, K. Goushi, K. Shizu, H. Nomura and C. Adachi, *Nature*, 2012, **492**, 234; (b) T. Hatakeyama, K. Shiren, K. Nakajima, S. Nomura, S. Nakatsuka, K. Kinoshita, J. Ni, Y. Ono and T. Ikuta, *Adv. Mater.*, 2016, **28**, 2777; (c) L. Wan, Z. Cheng, F. Liu and P. Lu, *Mater. Chem. Front.*, 2023, **7**, 4420.
2 S. Sasaki, G. P. C. Drummen and G. Konishi, *J. Mater. Chem. C*, 2016, **4**, 2731.
3 (a) S. Yamaguchi, S. Akiyama and K. Tamao, *J. Am. Chem. Soc.*, 2001, **123**, 11372; (b) S. Yamaguchi and A. Wakamiya, *Pure Appl. Chem.*, 2006, **78**, 1413; (c) F. Jäkle, *Coord. Chem. Rev.*, 2006, **250**, 1107.
4 (a) A. A. Danopoulos, J. R. Galsworthy, M. L. H. Green, L. H. Doerrer, S. Cafferkey and M. B. Hursthouse, *Chem. Commun.*, 1998, 2529; (b) C. Bergquist, B. M. Bridgewater, C. J. Harlan, J. R. Norton, R. A. Friesner and G. Parkin, *J. Am. Chem. Soc.*, 2000, **122**, 10581.
5 (a) J. D. Hoefelmeyer and F. P. Gabbaï, *J. Am. Chem. Soc.*, 2000, **122**, 9054; (b) A. Hübner, A. M. Diehl, M. Diefenbach, B. Endeward, M. Bolte, H. Lerner, M. C. Holthausen and M. Wagner, *Angew. Chem., Int. Ed.*, 2014, **53**, 4832.
6 T. Tsukada, Y. Shoji, K. Takenouchi, H. Taka and T. Fukushima, *Chem. Commun.*, 2022, **58**, 4973.
7 J. M. Dos Santos, D. Hall, B. Basumatary, M. Bryden, D. Chen, P. Choudhary, T. Comerford, E. Crovini, A. Danos, J. De *et al.*, *Chem. Rev.*, 2024, **124**, 13736.
8 (a) E. R. Johnson, S. Keinan, P. Mori-Sánchez, J. Contreras-García, A. J. Cohen and W. Yang, *J. Am. Chem. Soc.*, 2010, **132**, 6498; (b) J. Contreras-García, E. R. Johnson, S. Keinan, R. Chaudret, J.-P. Piquemal, D. N. Beratan and W. Yang, *J. Chem. Theory Comput.*, 2011, **7**, 625.
9 J. N. Weiss, *The FASEB J.*, 1997, **11**, 835.
10 J. Coca, R. M. Diaz and C. Pazos, *Fluid Phase Equilibr.*, 1980, **4**, 125.
11 (a) M.A. Little and A. I. Cooper, *Adv. Funct. Mater.*, 2020, **30**, 1909842; (b) I. Senkovska, V. Bon, A. Mosberger, Y. Wang and S. Kaskel, *Adv. Mater.*, 2025, 2414724; (c) R. Mustafa, D. Diorio, M. Harper and D. Punihaole, *Soft Matter*, 2025, **21**, 4192; (d) K. Jie, Y. Zhou, E. Li and F. Huang, *Acc. Chem. Res.*,

2018, **51**, 2064; (e) F. Ishiwari, H. Hasebe, S. Matsumura, F. Hajjaj, N. Horii-Hayashi, M. Nishi, T. Someya and T. Fukushima, *Sci. Rep.*, 2016, **6**, 24275.

View Article Online
DOI: 10.1039/D5CC06166K

View Article Online
DOI: 10.1039/D5CC06166K

Data availability

All experimental details and data supporting this article are available in the supplementary information (SI).